Influence of Mean State Changes on the Structure of ENSO in a Tropical Coupled GCM

FRANCIS CODRON, AUGUSTIN VINTZILEOS, AND ROBERT SADOURNY

Laboratoire de Meteorologie Dynamique du CNRS, Paris, France

(Manuscript received 3 September 1999, in final form 6 March 2000)

ABSTRACT

This study examines the response of the climate simulated by the Institut Pierre Simon Laplace tropical Pacific coupled general circulation model to two changes in parameterization: an improved coupling scheme at the coast, and the introduction of a saturation mixing ratio limiter in the water vapor advection scheme, which improves the rainfall distribution over and around orography. The main effect of these modifications is the suppression of spurious upwelling off the South American coast in Northern Hemisphere summer. Coupled feedbacks then extend this warming over the whole basin in an El Niño–like structure, with a maximum at the equator and in the eastern part of the basin. The mean precipitation pattern widens and moves equatorward as the trade winds weaken.

This warmer mean state leads to a doubling of the standard deviation of interannual SST anomalies, and to a longer ENSO period. The structure of the ENSO cycle also shifts from westward propagation in the original simulation to a standing oscillation. The simulation of El Niño thus improves when compared to recent observed events. The study of ENSO spatial structure and lagged correlations shows that these changes of El Niño characteristics are caused by both the increase of amplitude and the modification of the spatial structure of the wind stress response to SST anomalies.

These results show that both the mean state and variability of the tropical ocean can be very sensitive to biases or forcings, even geographically localized. They may also give some insight into the mechanisms responsible for the changes in ENSO characteristics due to decadal variability or climate change.

1. Introduction

Interactions between the ocean and the atmosphere play a great role in the tropical Pacific climate on a wide range of timescales, from the diurnal, intraseasonal (Wang and Xie 1998) to seasonal cycle and interannual variability.

Since Bjerknes (1969), ENSO has been viewed as a coupled phenomenon, although several mechanisms may explain the growth and oscillation of anomalies (Neelin et al. 1998). Coupled processes are also thought to amplify the eastern equatorial Pacific seasonal cycle and explain its westward propagation (Li and Philander 1996; Chang 1996; Nigam and Chao 1996). Xie (1994) and Xie and Philander (1994) proposed a wind-evaporation feedback to explain the ITCZ position north of the equator and the maintaining of the underlying warm SST band. Several GCM studies also demonstrated the importance of the shape of the coastline (Philander et al. 1996), stratocumulus cloud decks (Yu and Mechoso 1999), and vertical mixing (Koberle and Philander 1994) and solar penetration (Schneider and Zhu 1998) in the ocean, in determining both the mean state and seasonal cycle. In the zonal direction, Neelin and Dijkstra (1995) showed using a simple model that given a small, uniform, externally forced mean upwelling, coupled feedbacks could yield a realistic climatology for the SST, wind stress, and thermocline depth.

The tropical climate does not, however, evolve independently at these different frequencies. The ENSO cycle is phase locked on the annual cycle, with a tendency to peak toward the end of the year (Mitchell and Wallace 1996). This is one possible reason for ENSO chaotic behavior (Jin et al. 1994; Tziperman et al. 1994; Wang and Fang 1996). On the other hand, the seasonal cycle amplitude seems linked to the ENSO phase, with a stronger cycle during cold phases (Gu and Philander 1995). The space–time structure of ENSO also changes on longer timescales. Using wavelet and waveform analysis, Wang and Wang (1996) found that ENSO exhibits both amplitude and period changes, the less energetic periods being dominated by a quasi-biennial oscillation (QBO), while stronger events have a broader spectral peak at 3–7 yr. Both Wang (1995) and Zhang et al. (1998) looked at the Comprehensive Ocean–Atmo-

Corresponding author address: Dr. Francis Codron, Joint Institute for Study of Ocean and Atmosphere, University of Washington, Box 354235, Seattle, WA 98195-4235.
E-mail: codron@atmos.washington.edu

sphere Data Set (COADS) dataset back to 1950. Wang (1995) found that before the late 1970s, the warming at the South American coast occurred before the central Pacific warming, while the contrary was observed after the 1970s. He attributed this observation to a change in the background SST state. Zhang et al. (1998) related the westward-propagating behavior to the QBO and standing oscillation characteristics to the lower-frequency mode. The 1982 event even displayed eastward propagation.

The ENSO characteristics can be changed in simple and intermediate models by varying some parameters or the climatological mean state (Zebiak and Cane 1987; Battisti and Hirst 1989; Jin and Neelin 1993). Coupled general circulation models also exhibit very different El Niño behaviors (Neelin et al. 1992; Delecluse et al. 1998). Both Moore (1995) and Li and Hogan (1999) observed that the simulation of ENSO changed dramatically whether or not flux corrections were used in their GCMs. The mean state of the uncorrected simulation was, however, far from the observed one. Studying the impact of a CO_2 doubling, Timmermann et al. (1999) found that ENSO was more energetic in the increased CO_2 simulation, in which the upper-tropical ocean is warmer and the thermocline sharper. The increase in El Niño events amplitude is attributed to a stronger response of SST to wind stress anomalies.

These issues are addressed using the Institut Pierre Simon Laplace (IPSL) coupled atmosphere–tropical Pacific GCM. A previous simulation was described by Vintzileos et al. (1999a,b), in which the mean state and the annual and interannual variability were quite realistic, despite some discrepancies near the eastern Pacific coast. To reduce these errors in a new simulation, changes were made in the coupling method at the coast and the water vapor advection scheme, which have a strong direct effect, but localized at the east coast. Coupled feedbacks are, however, able to modify the structure of the response, resulting in large basinwide differences in the simulated mean state. The interannual variability is in turn strongly affected by the changes in the background climatology. The mean state and ENSO sensitivity is thus largely due to adjustments of the coupled climate system, triggered by parameterization changes.

The rest of the paper is organized as follows. Section 2 gives the details of the coupled GCM, and describes the parameterization changes between the two simulations. The mean state and seasonal cycle sensitivity are analyzed in section 3. Section 4 describes the changes in the interannual variability structure and discusses the possible reasons. The main results are then summed up and discussed in section 5.

2. Model description

a. The coupled model

The atmospheric component of the IPSL tropical coupled model is version 5b of the Laboratoire de Météorologie Dynamique gridpoint GCM, close to the one described by Harzallah and Sadourny (1995). Its main features are summarized in Table 1. The horizontal resolution is 64 × 50 points equally spaced in longitude and sine of latitude, which provides a better meridional resolution in the Tropics. The vertical structure involves 11 layers.

TABLE 1. LMD AGCM characteristics.

Horizontal resolution	64 long × 50 sine of lat
Horizontal advection	Upstream scheme
Dynamic equations	Sadourny (1975)
Lateral diffusion	bi-Laplacian
Vertical coordinate	11 layers in $\sigma = p/p_s$
Thermodynamic variable	Potential enthalpy $H = C_pT\,(p_s/p)^{\kappa}$
Shortwave radiation	Fouquart and Bonnel (1980)
Longwave radiation	Morcrette (1991)
Clouds parameterization	Le Treut and Li (1991)
Boundary layer	Bulk aerodynamic
Convection schemes	Manabe and Strickler (1964) saturated case; Kuo (1965) unsaturated case

The oceanic model is the GCM developed at Laboratoire d'Oceanographie Dynamique et de Climatologie (Andrich et al. 1988). The domain covers the tropical Pacific between 47°S and 50°N. The horizontal resolution is 0.75° in longitude, in the meridional direction it extends from 0.33° near the equator to 1.5° at the boundaries. In the ocean interior, temperature and salinity are restored toward climatological values (Levitus 1982) to account for the heat and salt fluxes through the meridional boundaries. The restoring coefficient decreases to 0 at the equator and at the coasts. It is equal to one-fourth of its maximum value at ±10° from the equator, and only one-fifteenth at ±5°. On the vertical it increases from 0 at the surface to 13 $days^{-1}$ at 150 m, then decreases to 2 yr^{-1} at the bottom.

The two models are coupled using the delocalized physics method developed by Vintzileos and Sadourny (1997) in which the physical parameterizations of the atmospheric model are computed on vertical columns based on the ocean model grid, thus allowing a better representation of nonlinear effects. The information exchange takes place every hour, that is, every ocean model time step.

Climatological SSTs (Reynolds and Marsico 1993) are prescribed over oceanic areas not covered by the model. To avoid discontinuities at the meridional boundaries of the ocean model, the heat flux received by the ocean is corrected outside of the 20°S–20°N band, reaching 40 W m^{-2} K^{-1} at the boundaries. The simulations start with an ocean at rest with climatological temperature and salinity. The atmosphere is initialized from a previous run on 1 January 1986. The first year of each simulation is removed before analysis to account for the model adjustment.

b. Changes in the parameterizations

The first experiment, designed Ctl, lasts for 30 yr. The corresponding simulated climate is described by Vintzileos et al. (1999a,b). The new simulation called Mod also lasts for 30 yr, and includes two modified parameterizations.

The delocalized physics method necessitates to interpolate the atmospheric variables on the ocean model grid before computing the physical tendencies. The interpolation scheme used in Vintzileos et al. (1999a,b) yielded reasonably smooth interpolated fields; however, near the coasts the use of information from continental atmospheric grid points to calculate values over the neighboring ocean model points lead to some errors. The different heat capacities of ocean and land mean that the surface air temperature can produce sharp gradients at the coast. A smooth interpolation scheme will yield erroneous temperatures over the ocean, which influences the surface fluxes both directly and through the dependence of the exchange coefficient on vertical stability. The interpolation scheme was thus modified to allow discontinuities in the interpolated fields near the coast, as described by Codron et al. (2000). It remains, however, identical in the ocean interior.

The most important modification concerns the horizontal water vapor advection scheme: moisture can be advected up mountain slopes along the terrain-following coordinates from a warm grid point to a much colder one. In reality, if supersaturation occurs on the way, the advected water vapor partly precipitates before reaching the summit. But if the temperature difference is not taken into account by the advection scheme, all the moisture reaches the colder point, leading to an systematic displacement of rainfall toward mountains tops. The resulting latent heat release in turn brings more air convergence over mountains, thereby enhancing the error. A simple way to correct this bias is to limit the advected water vapor to the downstream saturation value. The precipitation then occurs rather along the slopes, leading to much more realistic simulated patterns. The details of the modified schemes and the simulated precipitation sensitivity are the subject of a future paper.

3. Mean state and seasonal cycle

Water vapor advection is not much modified over the ocean by the introduction of the saturation limiter (section 2), because horizontal temperature gradients are relatively weak. This modification has, however, a strong effect in the eastern Pacific. Figure 1 shows the Northern Hemisphere winter precipitation over South America in the two simulations, together with the 850-hPa circulation. The rainfall maxima in Ctl are situated over the Andes summits and the Brazilian Plateau. The Mod field is smoother, and the Andes extremum is shifted over the slopes to the northeast. An important change in the wind field is the disappearance in Mod of a cyclonic circulation over the eastern Pacific between the equator and 15°S, forced in Ctl by the latent heating due to orographic precipitation. The wind stress associated with this spurious circulation causes both Ekman pumping and strong evaporation and mixing between 5° and 10°S in Ctl, leading to cold SSTs that are then advected equatorward.

The mean equatorial Pacific SST for runs Ctl and Mod, and their difference are shown in Fig. 2. The cold patch near 5°S, 85°W in Ctl due to the spurious winter upwelling has disappeared in Mod. The warming is however not limited to the eastern Pacific, and has spread over most of the basin, into an El Niño–like structure with maximum amplitude at the equator and a meridional extent increasing eastward.

The thin band of cooler in Mod SST at the South American coast is the signature of the improved interpolation scheme. If the new interpolation scheme is introduced alone with no change in water vapor advection, this cooling extends westward along the equator with an amplitude of 0.5° (Codron et al. 2000). In Mod, it reduces the SST warming by approximately the same amount.

Comparison with the observed SSTs from Reynolds and Marsico (1993) in Fig. 3 shows that the western Pacific warm pool extent is better simulated in Mod. The cooling at the east coast is also an improvement. The simulated SSTs remain however too warm in the eastern Pacific, a probable cause being the lack of stratus clouds. The cooler SST in Ctl around 5°S, 85°W may appear more realistic, but it happens at the wrong time in the year, as shown below.

The differences in wind and precipitation, shown in Fig. 4, are consistent with the SST differences. The reduced zonal and meridional gradients and the warmer SST cause weakened eastward wind and increased convergence in Mod, in equilibrium with a widening of the ITCZ toward the equator and an eastward widening of the South Pacific Convergence Zone.

Seasonal cycle

The seasonal cycle of equatorial SST is shown in Fig. 5 for the Ctl and Mod simulations, and in Fig. 6 for the Reynolds observations. The phase of SST variations in the eastern Pacific in Mod is correct, as is the westward propagation tendency. The amplitude remains, however, weaker than observed, and the cold season does not last long enough in autumn. The SST seasonal cycle of the Ctl simulation is contaminated by strong errors within 15° from the eastern coast, resulting in a small amplitude and an important semiannual component.

4. Interannual variability

a. Temporal structure

The changes in the mean state and seasonal cycle have a very strong impact on the simulated interannual var-

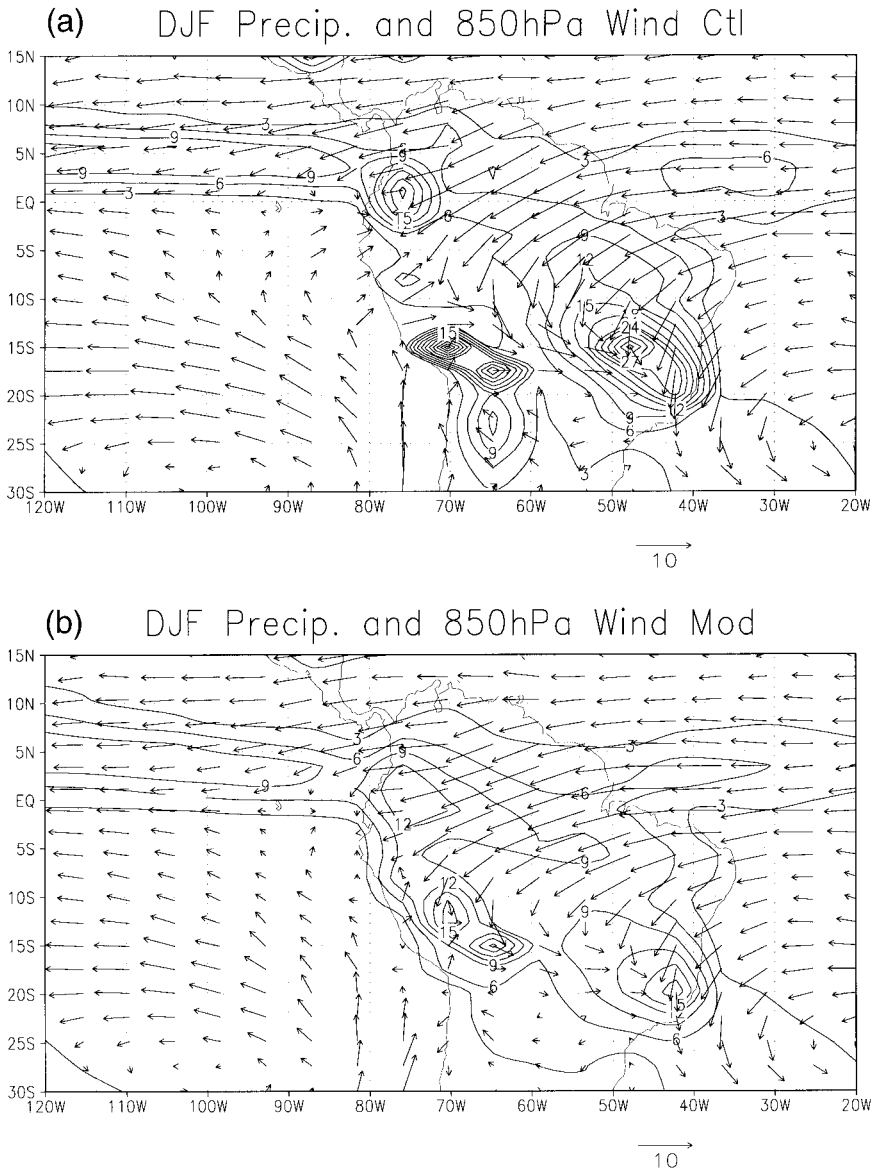

FIG. 1. Dec–Jan–Feb mean precipitation (mm day^{-1}) and 850-hPa wind over South America: (a) Ctl experiment and (b) Mod experiment.

iability. Figure 7 displays the time series of the interannual anomalies of the SST averaged over the Niño-3 box (2°S–2°N, 150°–90°W) for the last 29 yr of Ctl and Mod. The anomalies are defined relatively to the mean seasonal cycle of Ctl and Mod, respectively.

It is clear that the amplitude of El Niño events is greater in the new version, indeed the standard deviation of the anomalies is 0.8°C in Mod, instead of 0.37°C in Ctl. The periodicity is also modified: the Ctl simulation is dominated by QBO (Vintzileos et al. 1999b) whereas in Mod, the period between two events varies from 3 to 7 yr.

Another important change is the phase lock of ENSO on the annual cycle. The mean seasonal cycle of the Niño-3 SST for the Ctl and Mod simulations is plotted in Fig. 8 together with the standard deviation for each month of interannual anomalies. The annual mean has been removed everywhere. The fluctuations of the interannual anomalies standard deviation in Mod have a strong amplitude, and are in almost perfect phase opposition with the SST seasonal cycle. The situation is quite different in the Ctl simulation. The seasonal cycle of SST is about twice as weak as in Mod, because the spurious Southern Hemisphere coastal upwelling in winter opposes the annual warming of equatorial SST in spring. This strong upwelling can also bring to the surface subsurface temperature anomalies that are then advected to the equator. This explains why the monthly

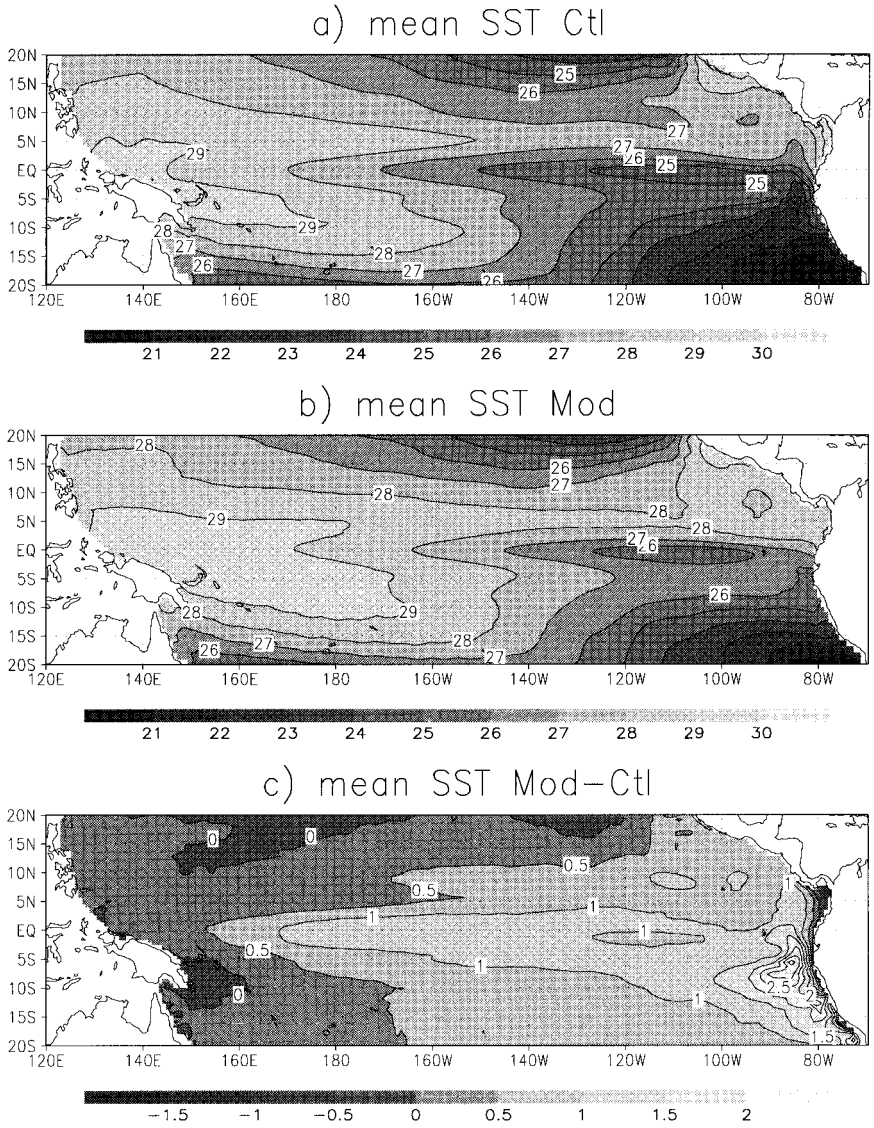

FIG. 2. Mean SST for runs (a) Ctl, and (b) Mod, and (c) their difference. The first year has been suppressed.

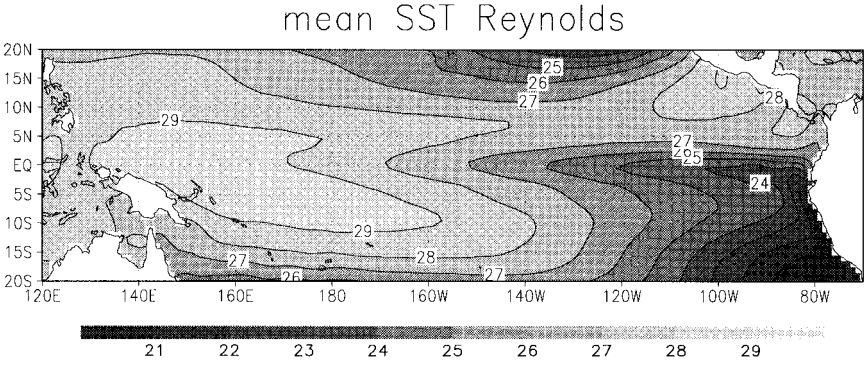

FIG. 3. Mean SST for the observed Reynolds dataset 1982–95.

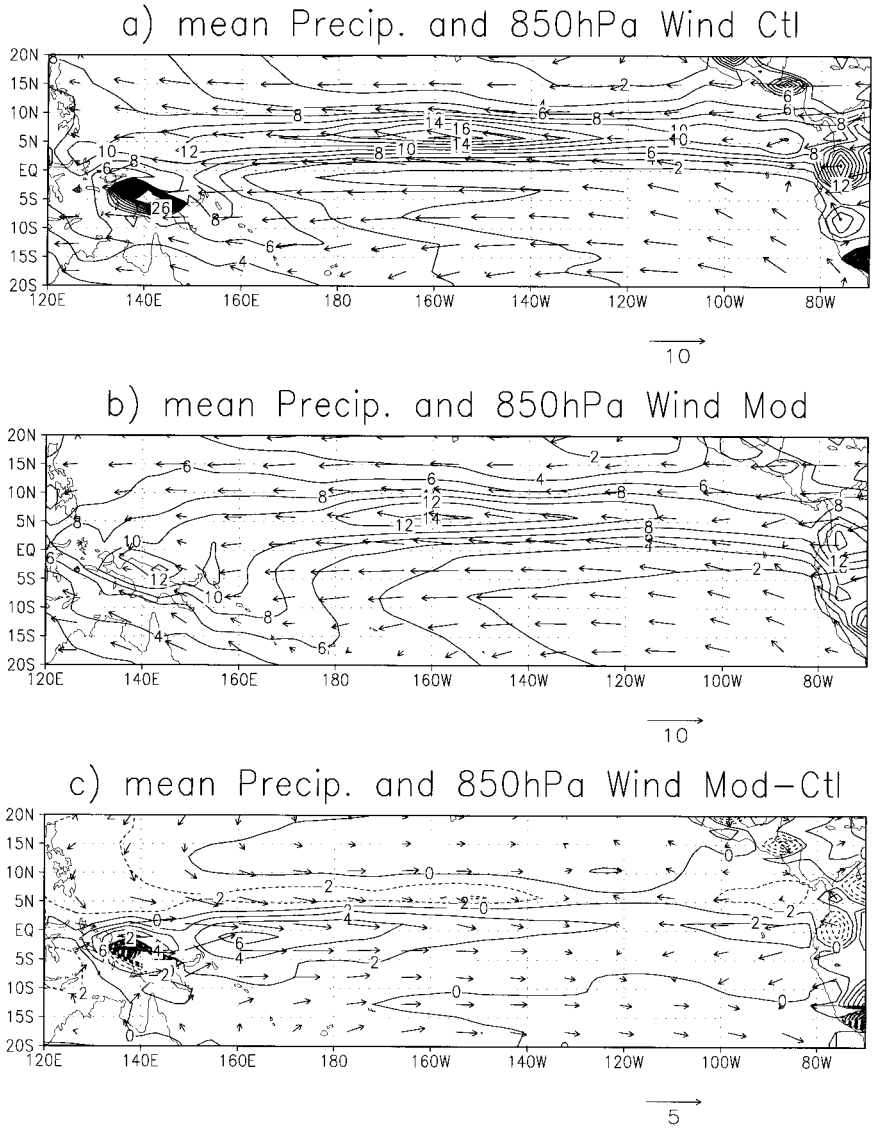

FIG. 4. Mean precipitation (contour) and 850-hPa wind (arrows) for runs (a) Ctl, and (b) Mod, and (c) their differences. Precipitation is in mm day^{-1}, and the wind is in m s^{-1}. The first year has been suppressed.

standard deviation in Ctl has a second maximum in spring and overall weak variations. These results suggest that in the IPSL model, El Niño tends to peak during parts of the year when the mean upwelling is strongest.

b. Spatial structure

Hovmuller diagrams of the evolution of interannual SST anomalies at the equator for simulations Ctl and Mod are shown in Fig. 9. The greater amplitude and longer duration of ENSO events in Mod is again evident. SST anomalies display a westward-propagation tendency in the Ctl simulation, apparent for example in years 1990–95. In Mod, SST anomalies behave more like a standing oscillation.

The spatial patterns associated with ENSO variability are constructed by regressing the global fields on the Niño-3 index time series, as in Wallace et al. (1998). The Niño-3 region is the area of maximum variance (together with the Peruvian coast) in both the Ctl and Mod simulations. The results shown are thus similar to those obtained by an EOF analysis, for example, by Vintzileos et al. (1999b) for the Ctl simulation. Figure 10 shows the regression fields for observed data during the tropical ocean and global atmosphere period January 1982–December 1992. We use Reynolds SST (Reynolds and Marsico 1993), Microwave Sounding Unit precip-

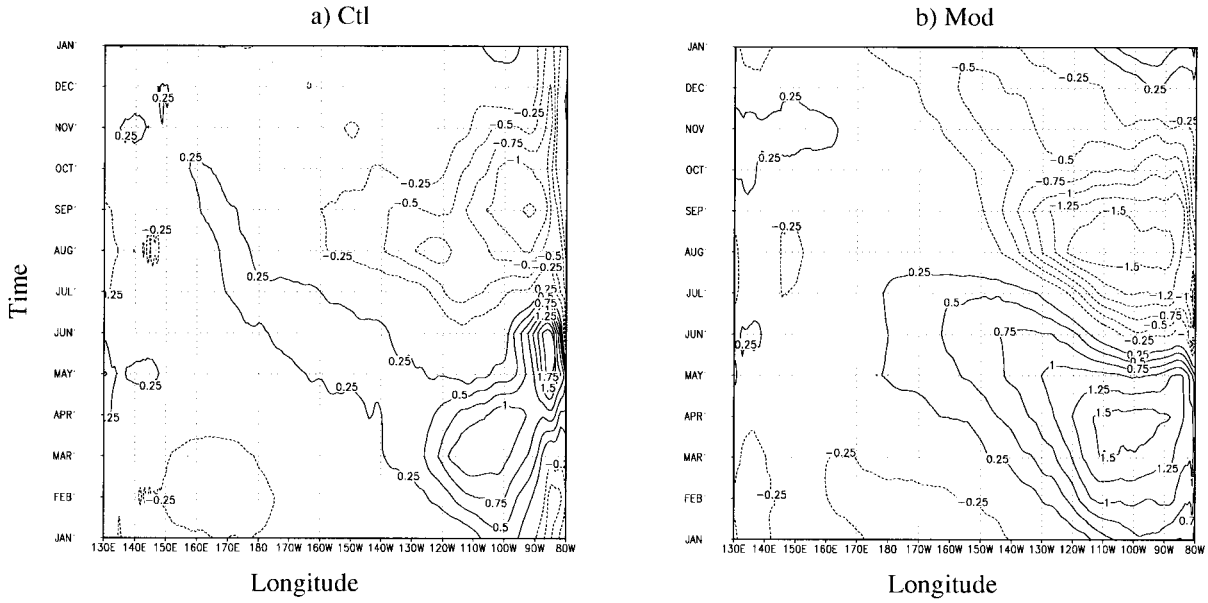

FIG. 5. Mean equatorial (2°S–2°N) SST seasonal cycle, annual mean removed: (a) Ctl simulation and (b) Mod simulation.

itation (Spencer 1993), and Florida State University pseudo–wind stress (Stricherz et al. 1992, 1997).

The patterns for the Ctl and Mod simulations are displayed in Figs. 11 and 12, respectively. The structures for the Ctl simulation tend to be too much zonal. The SST pattern is too narrow in latitude and extends almost all the way to the western border. The ITCZ band moves southward during El Niño, but there is little rainfall difference just on the equator; the SST there must remain under the threshold for convection. The precipitation increase during El Niño over the New Guinea region is also unrealistic. The band of westerly wind stress anomalies is very confined near the equator. There is even a reversal of the direction of zonal wind stress anomalies between 5° and 10°N, with anomalous easterly stress during El Niño. This reversal is not found in the observations: anomalous wind stress north of the equator is directed southward and has little zonal component.

The regression patterns for the warmer Mod simulation resemble much more the observed ones. SST anomalies have a wider meridional structure, and extend westward only to 170°E. The maximum in rainfall increase during El Niño is centered on the equator in the

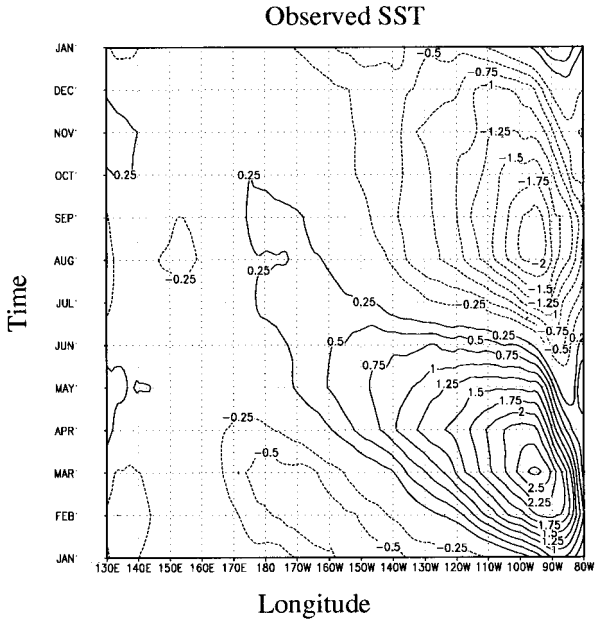

FIG. 6. Mean equatorial (2°S–2°N) SST seasonal cycle for Reynolds dataset (1982–95) annual mean removed.

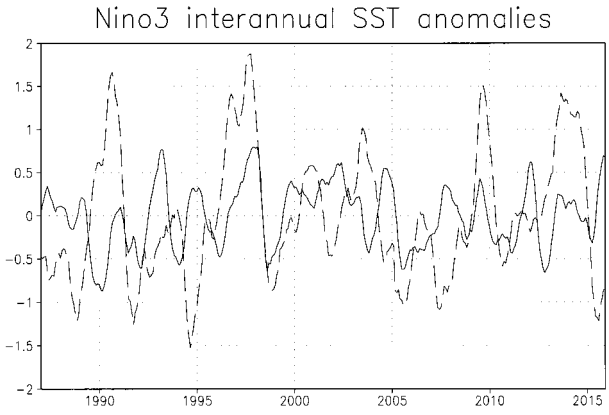

FIG. 7. Time series of the interannual anomalies of SST averaged over the box 2°S–2°N, 150°–90°W. Continuous line: Ctl run; dashed line: Mod run. The series have been smoothed by a 5-months' running mean.

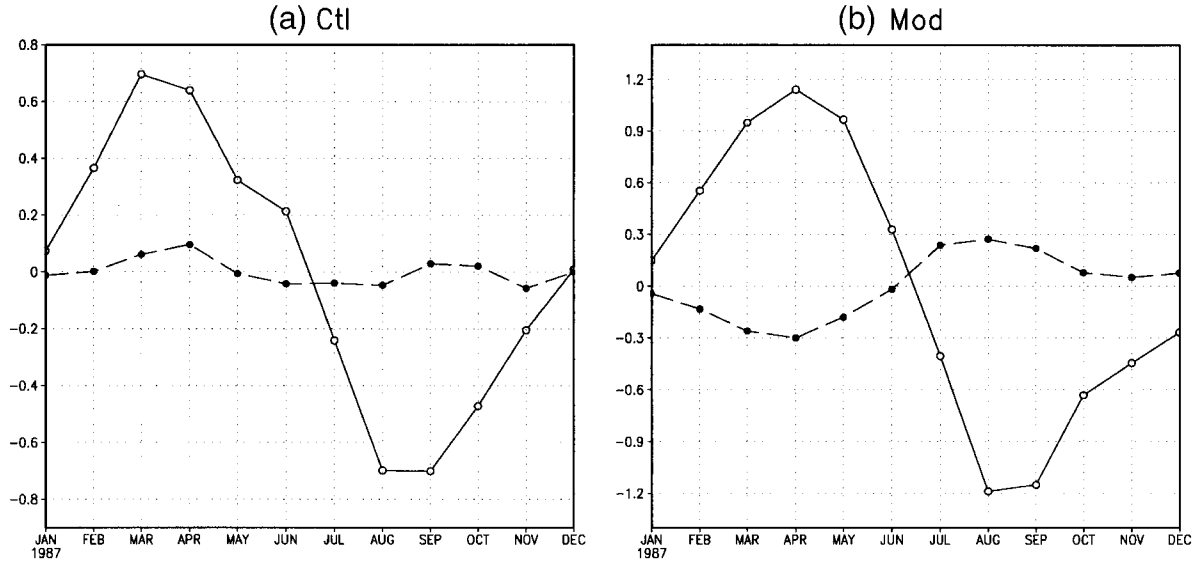

FIG. 8. Seasonal cycle of Niño-3 SST (continuous line) and monthly standard deviation of interannual anomalies (dashed line), for (left) Ctl and (right) Mod. The annual mean SST and standard deviation for each simulation has been removed.

central Pacific, and there is also significant increase to the south. The western Pacific is a region of precipitation decrease, as in the MSU observations. The anomalous wind stress pattern is also more realistic: the westerlies cover a broader range of latitude than in Ctl, and are more confined to the central-west Pacific in the zonal direction. The Mod simulation is able to capture the extension of westerly anomalies in the Southern Hemisphere between 160°E and 140°W, and the southerlies to the south.

c. Coupled feedbacks sensitivity

ENSO arises as a result of a feedback loop between SST, the wind stress, and the thermocline depth at the equator. To understand the increased amplitude of interannual variability in Mod, the different components of this loop are now examined.

The sensitivity of the anomalous equatorial zonal wind stress to unit SST interannual anomalies is first checked by calculating a linear regression on the Niño-3 SST: the covariance of the wind stress and Niño-3 SST divided by the variance of Niño-3 SST. This sensitivity (in Pa per °C) is shown in Fig. 13 for Ctl and Mod. In the eastern Pacific, the zonal wind stress response is weak in both runs, and even slightly negative in Mod. It is another indication that El Niño is driven more by upwelling of anomalous temperatures than by anomalous upwelling in this region. The stronger response is centered around the date line in both runs, but the maximum is almost twice as strong in Mod.

The changes in the mean oceanic subsurface structure between Ctl and Mod can also have an influence on ENSO. The warmer surface layer and generally shallower thermocline lead to a better defined thermocline in Mod. However, in the eastern Pacific vertical movements of the thermocline yield almost identical subsurface temperature anomalies in both runs, of 1°C per 10-m change. The mean thermal vertical structure thus does not seem to have a significant influence here. A possible explanation is that ENSO tends to peak in periods of the year when the equatorial upwelling is strong and the upper ocean is well mixed. These are also the seasons when there is the least difference between Ctl and Mod. For the seasonal cycle simulation on the other hand, the anomalous upwelling of the mean stratification is important (Koberle and Philander 1994), so the vertical structure may have more influence.

To close the feedback loop, we examine the influence of the wind stress anomalies on thermocline depth. A convenient way to look at the equatorial thermocline structure is to divide it into a zonal mean $\langle h \rangle$ and an east–west tilt h_x (zonal derivative of h). On ENSO timescales, the thermocline tilt is almost in equilibrium with the zonal wind stress due to the fast adjustment by Kelvin waves. Changes in this tilt may lead to surface temperature anomalies in the east where the mean thermocline is shallow. Part of the thermocline response is however not in steady balance with the wind stress, as demonstrated by Schneider et al. (1995), who forced an oceanic GCM with an observed wind stress time series, then with the same wind stress reversed in time. The ocean memory, necessary for oscillations, lies in this unbalanced response that depends on the wind stress history. Although it adjusts slowly to the wind stress forcing, the equatorial part of the ocean memory is almost constant in the zonal direction, still due to fast Kelvin waves.

Anomalous equatorial westerlies will deepen the thermocline in the east by increasing h_x, yielding a positive

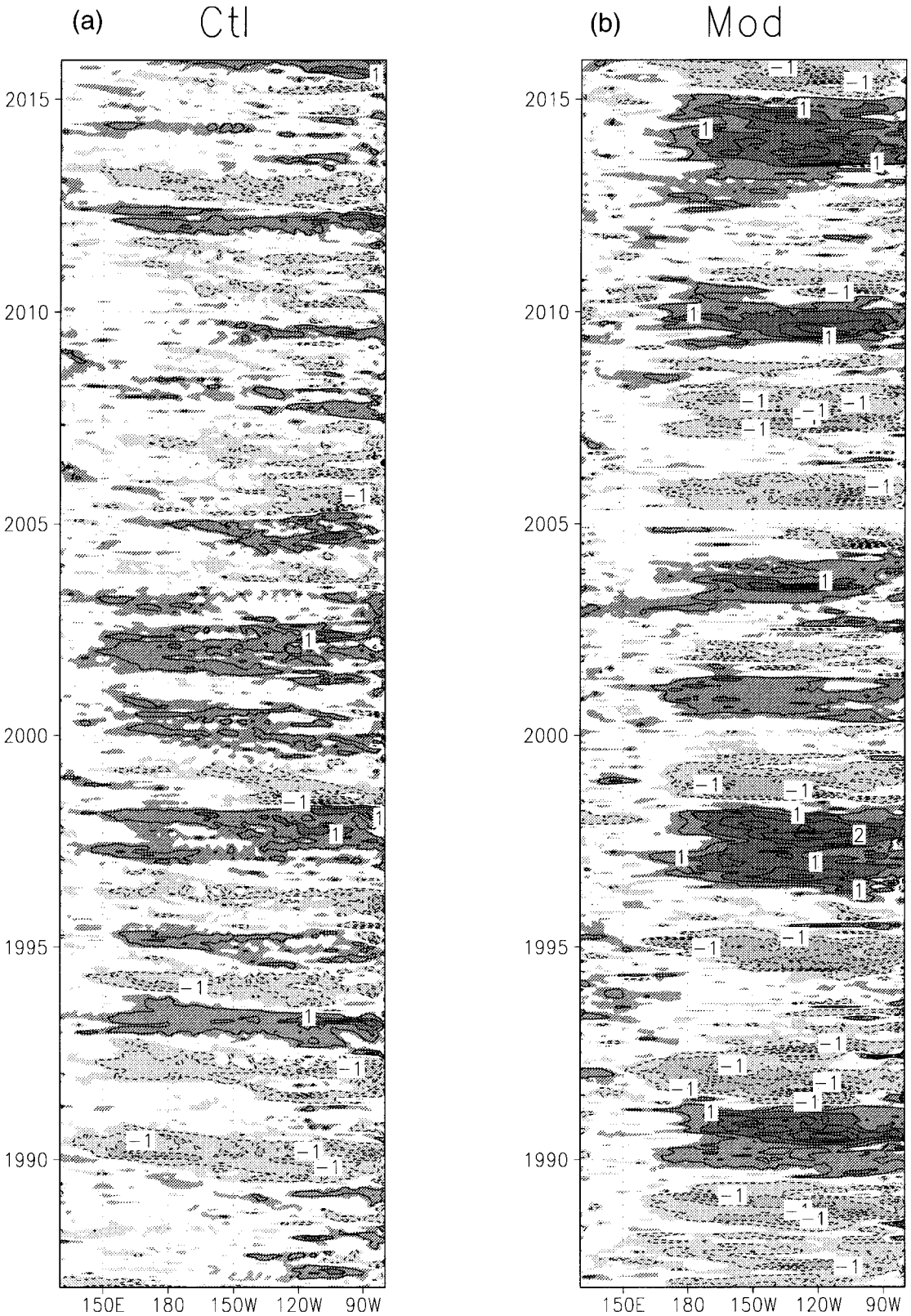

FIG. 9. Longitude–time diagram of interannual equatorial (2°S–2°N) SST anomalies, for (left) Ctl and (right) Mod. Contours every 0.5° C. Shading above 0.25° and 2°C. Light shading denotes cold anomalies; dark shading warm anomalies.

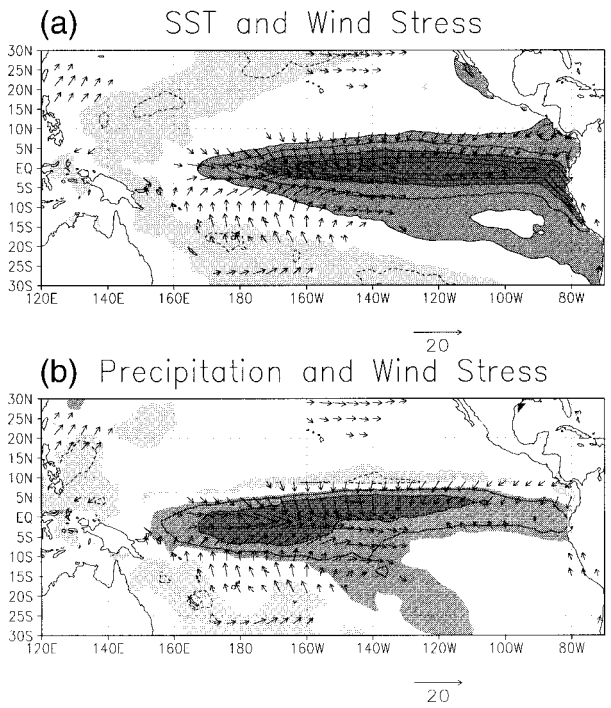

FIG. 10. Linear regressions on the Niño-3 SST index for the period Jan 1982–Dec 1992. Units are per 1°C Niño-3 anomaly. (a) Reynolds SST and FSU pseudo–wind stress. Contours every 0.2, light shading for SST anomalies below −0.1, heavy shading above 0.2 and 0.6. Only wind vectors of magnitude above 3 $m^2\ s^{-2}\ °C^{-1}$ are plotted. (b) MSU rainfall and FSU pseudo–wind stress. Contours every 1 mm day^{-1} °C, light shading for anomalies under −0.5, heavy shading above 0.5 and 2.

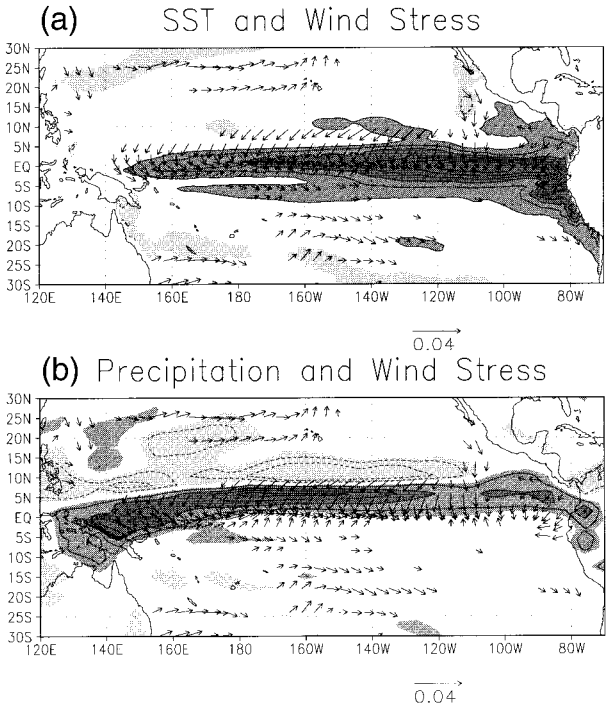

FIG. 11. Same as Fig. 10, for fields from the Ctl simulation. The Niño-3 time series is plotted in Fig. 7. Only wind stress vectors of magnitude above 0.006 Pa $°C^{-1}$ are plotted.

feedback on warm SSTs. Simultaneously, $\langle h \rangle$ will slowly decrease, eventually overwhelming the positive feedback. Several mechanisms may contribute to the mean thermocline adjustment. Westerlies yield off-equatorial upwelling, which forces upwelling westward-propagating Rossby waves. These waves may then reflect into Kelvin waves when they reach the western boundary. This mechanism is essential to the ''delayed oscillator'' mechanism of Battisti and Hirst (1989). Vintzileos et al. (1999a,b) also showed in the Ctl simulation that the off-equatorial upwelling caused more ''draining'' of surface water toward higher latitudes, thereby weakening the meridional recirculation cells that bring water from the surface to the equator at the thermocline depth. The thermocline thus slowly shallows because of the meridional flow divergence. Schneider et al. (1994) demonstrated that in the fast Kelvin waves approximation, the time rate of change of the zonal mean thermocline depth $\langle h \rangle$ is proportional to the meridional gradient of the zonal mean curl of the wind stress at the equator. No explicit wave delay is needed in this mechanism. The sensitivity of h_x and $\langle h \rangle$ to anomalous central Pacific equatorial zonal wind stress is shown in Fig. 14 for lags from −6 to 6 months. The wind stress index is an average over the box 2°S–2°N, 160°E–150°W. The ther-

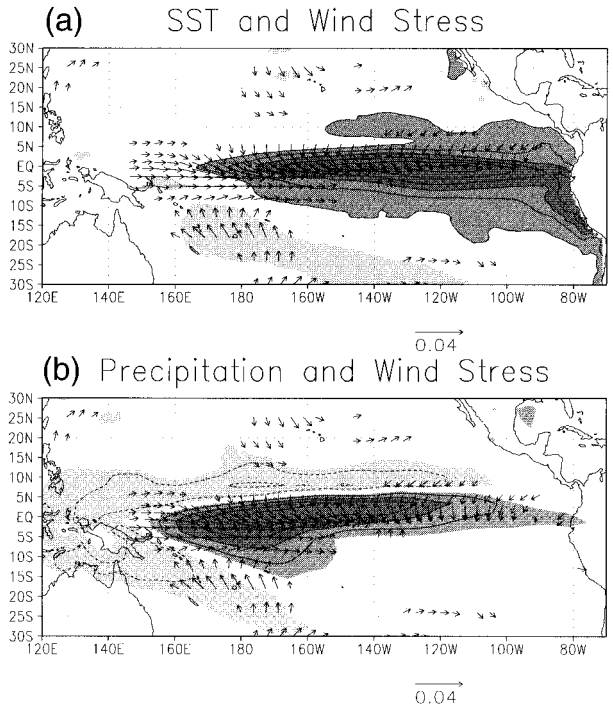

FIG. 12. Same as Fig. 10, for fields from the Mod simulation.

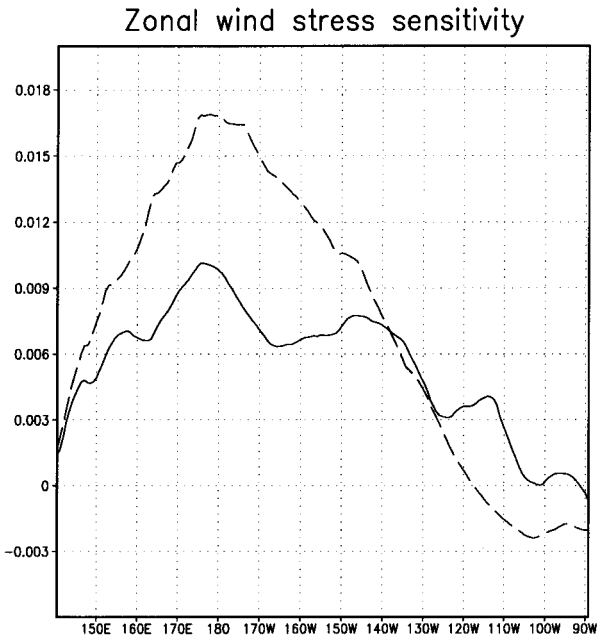

FIG. 13. Sensitivity of equatorial (2°S–2°N) zonal wind stress to Niño-3 SST, in Pa per °C. Continuous line: Ctl run; dashed line: Mod run. See text for definition.

mocline tilt sensitivity is maximum when h_x lags the wind forcing by about 1 month, and its value is identical in both runs. The sensitivity decays more rapidly in Ctl mainly because the lagged autocorrelation of interannual wind stress anomalies is weaker. On the other hand, $\langle h \rangle$ shifts from a deeper thermocline before the westerly anomaly to a shallower thermocline some months later.

The anomalous wind stress is thus almost in balance with h_x, and with the time derivative of $\langle h \rangle$, agreeing with the theory just developed. However, the change in $\langle h \rangle$ is much stronger in Ctl. The spatial structure of the wind stress response of Figs. 11 and 12 helps to understand why. For a same amplitude of equatorial westerlies, the wind stress curl north of the equator, which drives the upwelling, will be much higher in Ctl because of the strong westward wind stress north of 5°N. In Mod, the smoother wind stress meridional variation yields a curl also positive but weaker. The relatively stronger impact on $\langle h \rangle$ (yielding a negative feedback on SST anomalies) than on h_x (positive feedback) in Ctl may explain the smaller amplitude and shorter period of ENSO events.

5. Conclusions and discussion

The sensitivity of the tropical Pacific climate simulated by the IPSL coupled general circulation model to two parameterization changes has been studied. The model changes concern the atmosphere–ocean interpolation scheme near the coast, and the introduction of a saturation limiter in the water vapor advection scheme. Although the latter modification has a strong beneficial impact on the simulated rainfall, especially near orography, it has no direct effect over the ocean where horizontal temperature gradients are weaker than along mountain slopes. However, the reduction of spurious precipitation over the Andes in Northern Hemisphere winter lead to the disappearance of a cyclonic circulation in the southeastern Pacific, thus suppressing an anomalous upwelling off the South American coast. The

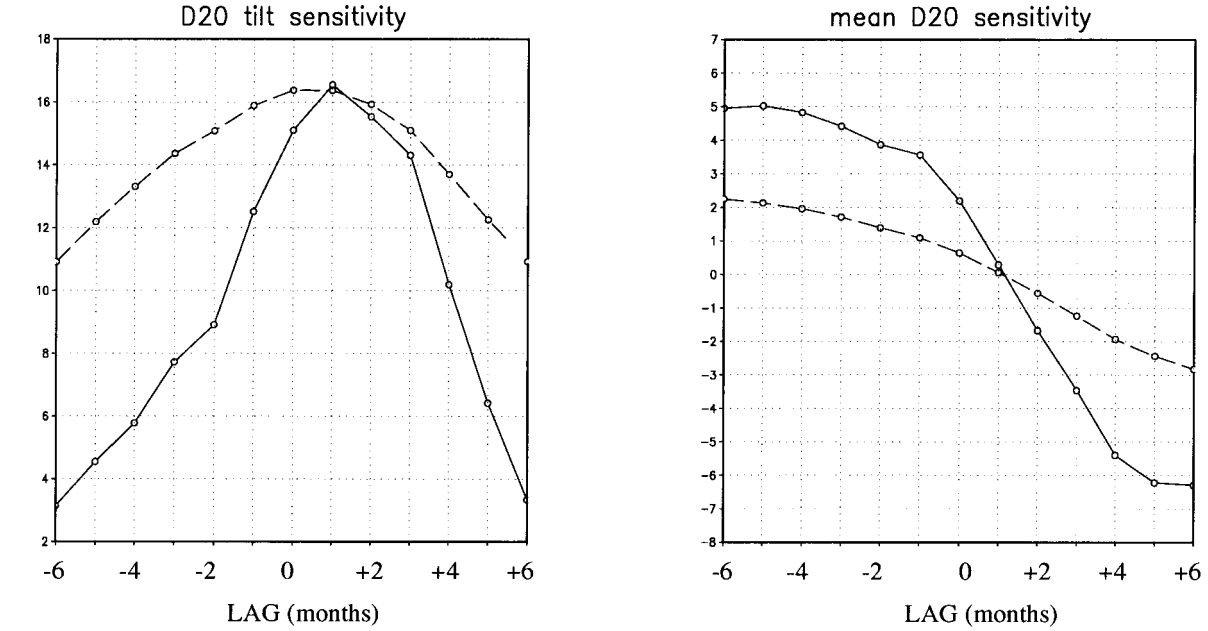

FIG. 14. Sensitivity of equatorial thermocline depth to central Pacific wind stress, in meters per 0.01Pa. (left) Thermocline tilt (east–west). (right) Mean thermocline depth. Ctl run is in continuous line, Mod run in dashed line. The wind stress leads the D20 for positive lags.

local ocean warming forced by the atmosphere near the coast is then able to propagate over the whole basin through coupled mechanisms. The final difference pattern has an El Niño–like structure with stronger differences at the equator and in the east. The area covered by the western Pacific warm SST pool, and the associated convergence and convection zone in the atmosphere, is much widened. The equilibrium of the tropical Pacific coupled system is thus shown to be very sensitive to a forcing difference, even though it is spatially confined.

The mean state warming has a considerable influence on the simulation of interannual variability. El Niño characteristics shift from a westward-propagating quasi-biennial oscillation in Ctl, to a standing oscillation with 3–6-yr periodicity; in addition, the amplitude in Mod is twice as large (standard deviation of 0.81°C instead of 0.37°C).

These changes in El Niño behavior are consistent with the observed fluctuations of El Niño on interdecadal timescales (Wang 1995; Zhang et al. 1998; Wang and Wang 1996; Torrence and Webster 1998). They are also strikingly similar to the results obtained by Kirtman and Schopf (1998) with an intermediate coupled model with weather noise forcing. Kirtman and Schopf (1998) found decadal changes in ENSO characteristics, with decades of high-amplitude, regular interannual variability, and decades of low-amplitude, high-frequency variability. The strong ENSO decades were characterized by higher than average SST in the central-eastern Pacific and weaker trades, much like the Mod − Ctl difference. It is important to understand how the mean state affects the ENSO structure, for predictability studies, and to predict ENSO behavior changes in a global warming context.

Several factors contribute to this enhancement of interannual variability. The sensitivity of the central-west Pacific equatorial wind stress to an eastern Pacific SST anomaly is stronger in the warmer climate of Mod, providing a bigger positive feedback on SST.

The spatial structure of the wind stress response is also different in the two simulations. In Ctl, the anomalous zonal wind stress has a zonal structure associated with the southward migration of the ITCZ during El Niño, whereas in Mod both the convection and wind stress response have a nonzonal structure centered near the equator in the west Pacific, with a wider meridional extent. These patterns force different responses of the thermocline depth. The strong off-equatorial wind stress curl in Ctl has a relatively stronger impact on the mean equatorial thermocline depth, a delayed negative feedback on SST anomalies, than on the east–west tilt that provides the positive feedback. We propose this effect as an explanation for the shorter ENSO period in Ctl.

Neelin (1991) showed that the relative phase of SST and wind anomalies in the zonal direction was important for ENSO evolution, with wind anomalies to the west of SST favoring westward propagation, while superposed anomalies lead to eastward propagation. He did not, however, take into account variations of the mean thermocline depth, for which the meridional structure of the wind stress response is important. This parameter was included in some recent simple models of ENSO by Jin (1997) and Li (1997).

The intraseasonal variability was not studied in this paper, but may also play a role in the ENSO modification. Torrence and Webster (1998) suggested that the observed weak persistence of ENSO in the spring is due to a low signal-to-noise ratio, where signal means interannual anomalies, and the noise is the effect of short timescale wind variability, as westerly wind bursts, on SST. The wind stress ''noise'' level, that is, the variance at intraseasonal timescales, is equivalent in the Mod and Ctl runs. The variance on interannual timescales is however 4 times greater in Mod. The higher signal-to-noise ratio in Mod can reinforce the longer characteristic persistence of anomalies.

Acknowledgments. The numerical experiments have been conducted at IDRIS (Institut de Développement et de Recherches en Informatique Scientifique) of the Centre National de la Recherche Scientifique. The authors would like to thank the two anonymous reviewers who made helpful comments on a preliminary version of this paper.

REFERENCES

Andrich, P., P. Delecluse, C. Levy, and G. Madec, 1988: A multitasked general circulation model of the ocean. *Science and Engineering on Cray Supercomputers, Proceedings of the Fourth International Symposium*, Cray Research Inc., 407–428.

Battisti, D. S., and A. C. Hirst, 1989: Interannual variability in a tropical atmosphere–ocean model: Influence of the basic state, ocean geometry, and nonlinearity. *J. Atmos. Sci.*, **46,** 1687–1713.

Bjerknes, J., 1969: Atmospheric teleconnections from the equatorial Pacific. *Mon. Wea. Rev.*, **97,** 163–172.

Chang, P., 1996: The role of the dynamic ocean–atmosphere interactions in the tropical seasonal cycle. *J. Climate*, **9,** 2973–2985.

Codron, F., A. Vintzileos, and R. Sadourny, 2000: An improved scheme for interpolation between an atmospheric model and underlying surface grids near orography and ocean boundaries. *Mon. Wea. Rev.*, **128,** 1177–1186.

Delecluse, P., M. Davey, Y. Kitamura, S. G. H. Philander, M. Suarez, and L. Bengtsson, 1998: Coupled general circulation modeling of the tropical Pacific. *J. Geophys. Res.*, **103** (C7), 14 357–14 373.

Fouquart, Y., and B. Bonnel, 1980: Computation of solar heating of the earth's atmosphere: A new parametrization. *Beitr. Phys. Atmos.*, **53,** 35–62.

Gu, D., and S. G. H. Philander, 1995: Secular changes of annual and interannual variability in the Tropics during the past century. *J. Climate*, **8,** 864–876.

Harzallah, A., and R. Sadourny, 1995: Internal versus SST-forced atmospheric variability as simulated by an atmospheric general circulation model. *J. Climate*, **8,** 474–495.

Jin, F. F., 1997: An equatorial ocean recharge paradigm for ENSO. Part I: Conceptual model. *J. Atmos. Sci.*, **54,** 811–829.

——, and J. D. Neelin, 1993: Modes of interannual tropical ocean–atmosphere interaction—A unified view. Part I: Numerical results. *J. Atmos. Sci.*, **50,** 3477–3503.

——, ——, and M. Ghil, 1994: El Niño on the devil's staircase: Annual subharmonic steps to chaos. *Science,* **263,** 70–72.
Kirtman, B. P., and P. S. Schopf, 1998: Decadal variability in ENSO predictability and prediction. *J. Climate,* **11,** 2804–2822.
Koberle, C., and S. G. H. Philander, 1994: On the processes that control seasonal variations of sea surface temperatures in the tropical Pacific Ocean. *Tellus,* **46A,** 481–496.
Kuo, H., 1965: On formation and intensification of tropical cyclones through latent heat release by cumulus convection. *J. Atmos. Sci.,* **22,** 40–63.
Le Treut, H., and Z.-X. Li, 1991: Sensitivity of an atmospheric general circulation model to prescribed SST changes: Feedback effects associated with the simulation of cloud optical properties. *Climate Dyn.,* **5,** 175–187.
Levitus, S., 1982: *Climatological Atlas of the World Ocean.* NOAA Professional Paper 13, 173 pp.
Li, T., 1997: Phase transition of the El Niño–Southern Oscillation: A stationary SST mode. *J. Atmos. Sci.,* **54,** 2872–2887.
——, and S. G. H. Philander, 1996: On the annual cycle of the eastern equatorial Pacific. *J. Climate,* **9,** 2986–2998.
——, and T. F. Hogan, 1999: The role of the annual-mean climate on seasonal and interannual variability of the tropical Pacific in a coupled GCM. *J. Climate,* **12,** 780–792.
Manabe, S., and R. Strickler, 1964: Thermal equilibrium of the atmosphere with a convective adjustment. *J. Atmos. Sci.,* **21,** 361–385.
Mitchell, T. P., and J. M. Wallace, 1996: ENSO seasonality: 1950–78 versus 1979–92. *J. Climate,* **9,** 3149–3161.
Moore, A. M., 1995: Tropical interannual variability in a global coupled GCM: Sensitivity to mean climate state. *J. Climate,* **8,** 807–828.
Morcrette, J. J., 1991: Radiation and cloud radiative properties in the ECMWF operational weather forecast model. *J. Geophys. Res.,* **96,** 9121–9132.
Neelin, J. D., 1991: The slow sea surface temperature mode and the fast-wave limit: Analytic theory for tropical interannual oscillations and experiments in a hybrid coupled model. *J. Atmos. Sci.,* **48,** 584–606.
——, and H. A. Dijkstra, 1995: Ocean–atmosphere interaction and the tropical climatology. Part II: Why the Pacific cold tongue is in the east. *J. Climate,* **8,** 1343–1359.
——, and Coauthors, 1992: Tropical air–sea interaction in general circulation models. *Climate Dyn.,* **7,** 73–104.
——, D. S. Battisti, A. C. Hirst, F.-F. Jin, Y. Wakata, T. Yamagata, and S. E. Zebiak, 1998: ENSO theory. *J. Geophys. Res.,* **103** (C7), 14 261–14 290.
Nigam, S., and Y. Chao, 1996: Evolution dynamics of tropical ocean–atmosphere annual cycle variability. *J. Climate,* **9,** 3187–3205.
Philander, S. G. H., D. Gu, D. Halpern, G. Lambert, N.-C. Lau, T. Li, and R. C. Pacanowski, 1996: Why the ITCZ is mostly north of the equator. *J. Climate,* **9,** 2958–2972.
Reynolds, R. W., and D. C. Marsico, 1993: An improved real-time global sea surface temperature analysis. *J. Climate,* **6,** 114–119.
Sadourny, R., 1975: The dynamics of finite-difference models of the shallow-water equations. *J. Atmos. Sci.,* **32,** 680–689.
Schneider, E. K., and Z. Zhu, 1998: Sensitivity of the simulated annual cycle of sea surface temperature in the equatorial Pacific to sunlight penetration. *J. Climate,* **11,** 1932–1950.
——, B. Huang, and J. Shukla, 1994: Ocean wave dynamics and El Niño. COLA, Tech. Rep. 1, 4041 Powder Mill Rd., Suite 302, Calverton, MD 20705-3106, 46 pp. [Available from COLA,
——, ——, and ——, 1995: Ocean wave dynamics and El Niño. *J. Climate,* **8,** 2415–2439.
Spencer, R. W., 1993: Global oceanic precipitation from the MSU during 1979–91 and comparison to other climatologies. *J. Climate,* **6,** 1301–1326.
Stricherz, J., J. J. O'Brien, and D. M. Legler, 1992: *Atlas of Florida State University. Tropical Pacific Winds for TOGA 1966–1985.* Florida State University, 275 pp.
——, D. M. Legler, and J. J. O'Brien, 1997: *TOGA Pseudo-Stress Atlas 1985–1994.* Vol. II, *Pacific Ocean,* Florida State University, 155 pp.
Timmermann, A., J. Oberhuber, A. Bacher, M. Esch, M. Latif, and E. Roeckner, 1999: Increased El Niño frequency in a climate model forced by future greenhouse warming. *Nature,* **398,** 694–696.
Torrence, C., and P. J. Webster, 1998: The annual cycle of persistence in the El Niño/Southern Oscillation. *Quart. J. Roy. Meteor. Soc.,* **124,** 1985–2004.
Tziperman, E., L. Stone, M. Cane, and H. Jarosh, 1994: El Niño chaos: Overlapping of resonances between the seasonal cycle and the Pacific ocean–atmosphere oscillator. *Science,* **264,** 72–74.
Vintzileos, A., and R. Sadourny, 1997: A general interface between an atmospheric general circulation model and underlying ocean and land surface models: Delocalized physics scheme. *Mon. Wea. Rev.,* **125,** 926–941.
——, P. Delecluse, and R. Sadourny, 1999a: On the mechanisms in a tropical ocean–global atmosphere general circulation model. Part I: Mean state and the seasonal cycle. *Climate Dyn.,* **15,** 43–62.
——, ——, and ——, 1999b: On the mechanisms in a tropical ocean–global atmosphere general circulation model. Part II: Interannual variability and its relation to the seasonal cycle. *Climate Dyn.,* **15,** 63–80.
Wallace, J. M., E. M. Rasmusson, T. P. Mitchell, V. E. Kousky, E. S. Sarachik, and H. von Storch, 1998: On the structure and evolution of ENSO-related climate variability in the tropical Pacific: Lessons from TOGA. *J. Geophys. Res.,* **103,** 14 240–14 260.
Wang, B., 1995: Interdecadal changes in El Niño onset in the last four decades. *J. Climate,* **8,** 267–285.
——, and Z. Fang, 1996: Chaotic oscillations of tropical climate: A dynamic system theory for ENSO. *J. Atmos. Sci.,* **53,** 2786–2802.
——, and Y. Wang, 1996: Temporal structure of the Southern Oscillation as revealed by waveform and wavelet analysis. *J. Climate,* **9,** 1586–1598.
——, and X. Xie, 1998: Coupled modes of the warm pool climate system. Part I: The role of air–sea interaction in maintaining Madden–Julian oscillation. *J. Climate,* **11,** 2116–2135.
Xie, S.-P., 1994: Oceanic response to the wind forcing associated with the intertropical convergence zone in the northern hemisphere. *J. Geophys. Res.,* **99** (C10), 20 393–20 402.
——, and S. G. H. Philander, 1994: A coupled ocean–atmosphere model of relevance to the ITCZ in the eastern Pacific. *Tellus,* **46A,** 340–350.
Yu, J.-Y., and C. R. Mechoso, 1999: Links between annual variations of Peruvian stratocumulus clouds and of SST in the eastern equatorial Pacific. *J. Climate,* **12,** 3305–3318.
Zebiak, S. E., and M. A. Cane, 1987: A model El Niño–Southern Oscillation. *Mon. Wea. Rev.,* **115,** 2262–2278.
Zhang, X., J. Sheng, and A. Shabbar, 1998: Modes of interannual and interdecadal variability of Pacific SST. *J. Climate,* **11,** 2556–2569.